GPS-Inspired Stretchable Self-Powered Electronic Skin

Jinxin Zhang, Zijian Song, Hang Guo, Yu Song, Bocheng Yu, and Haixia Zhang

***Abstract*—Electronic skin has attracted much attention for their profound implications for human/machine interaction and medicine recently. To imitate the unique characteristics of skin, the electronic skin is moving towards stretchable, multifunctional, biodegradable, more sensitive and accurate. Here, we present a novel stretchable self-powered electronic skin, to detect the touch location in an analog method. Thanks to triboelectrification and planar electrostatic induction, the generation of location signals does not need an extra power supply. Inspired by Global Positioning System, the electronic skin has simple structure of a single layer poly(dimethylsiloxane) (PDMS) substrate and three carbon nanotube-PDMS (CNT-PDMS) composite electrodes, which not only reduce the electrode amount but also make the device stretchable. The less electrode number means the less fabrication cost, extra difficulties on electrode extraction, and in particular, less signal interference and data processing. Stretchability extends the application scenarios of the electronic skin to the curvilinear surfaces, such as cylindrical surfaces and spherical surfaces. Through special location method, the touch position can be read out easily and directly with averaged error sums of ∼1 mm. This new electronic skin takes a significant step forward in practical application.**

***Index Terms*—Electronic skin, stretchable electronics, self-powered, touch sensor.**

I. Introduction

AIMING at restoring the nature sense of skin to the people with skin damage or artificial intelligence and enhancing the human/machine interaction, the electronic skin has developed with the progress in a variety of new materials, structures and sensing methods [1]–[5]. Many electronic skins have the capability of detecting various sensation and transducing them to electrical signals, including temperature, strain, pressure, vibration, location, and humidity [6]–[9]. Such devices usually exhibit flexible, transparent, multifunctional, or skin like properties through the use of a diverse set of materials including but not limited to composites materials [10], [11], hydrogels [12], silicon nanomembranes [13], carbon nanotubes [14], 2D materials [15], organic semiconductors [16], etc. Resolution enhancement, energy conservation, stretchability and large area fabrication with low cost and high yield, however, are still the key issues that should be further developed to improve the performance of electronic skin and apply in reality [1], [12], [17], [18].

In previous works, precise position sensors mainly rely on the digital method that based on pixels [19], [20]. For digital electronic skin, the number of the sensing units or electrodes decides the resolution directly, which means that it is unavoidable to increase cost on electrodes, signal interference between pixels and data processing when improving the resolution. The analogue electronic skin could reduce measurement terminals significantly with sustaining the high resolution at the same time [12], [17]. Although flexible analog electronic skin can satisfy many requirements generated by the development of electronic skins, there is a problem that it can only work on flat surface [17]. It's crucial and indispensable to implement stretchable materials and structures to fully mimic the sensory of skin and expand applications.

For electronic skin based on capacitive or resistance system, a voltage should be on for the all-time to detect the change of the signal, which makes it a problem to supply power for electronic skin conveniently, steadily, sustainably and cheaply [12], [20]. The use of battery will increase the bulk, make it difficult to realize miniaturization and portable, and cause a serious problem of pollution [21]. Nanogenerators, such as triboelectric nanogenerator (TENG) and piezoelectric nanogenerator (PENG) [22]–[25], providing a potential choice to realize the self-powered system for its ability to transform mechanical energy into electrical power through triboelectrification and electrostatic induction or piezoelectricity. Many self-powered sensing systems based on nanogenerator have been developed in recent years, such as active mechanical sensors, environmental sensors and biomedical monitoring [26]–[34].

Here, we present an analogue electronic skin that can conformably integrate with curvilinear surfaces and even

Manuscript received December 9, 2017; revised February 19, 2018; accepted February 26, 2018. Date of publication February 28, 2018; date of current version May 8, 2018. This work was supported in part by the National Key Research and Development Program of China under Grant 2016YFA0202701, in part by the National Natural Science Foundation of China under Grant 61674004 and Grant 91323304, in part by the Beijing Science & Technology Project under Grant D151100003315003, and in part by the Beijing Natural Science Foundation of China under Grant 4141002. The review of this paper was arranged by Associate Editor Professor Xiaosheng Zhang. *(Jinxin Zhang and Zijian Song contributed equally to this work.) (Corresponding author: Haixia Zhang.)*

J. Zhang, Z. Song, Y. Song, and B. Yu are with the National Key Laboratory of Nano/Micro Fabrication Technology, Peking University, Beijing 100871, China (e-mail: jinxin.zhang@duke.edu; 49620300@qq.com; songyupku@pku.edu.cn; ybc@pku.edu.cn).

H. Guo is with the Academy for Advanced Interdisciplinary Studies, Peking University, Beijing 100871, China (e-mail: guohang@pku.edu.cn).

H. Zhang is with the National Key Laboratory of Nano/Micro Fabrication Technology, Peking University, Beijing 100871, China, and also with the Academy for Advanced Interdisciplinary Studies, Peking University, Beijing 100871, China (e-mail: zhang-alice@pku.edu.cn).

This paper has supplementary downloadable material available at http://ieeexplore.ieee.org, provided by the author.

Digital Object Identifier 10.1109/TNANO.2018.2810780

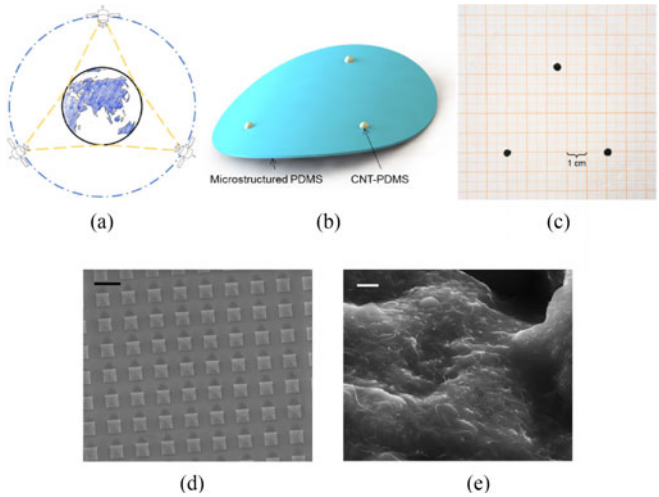

Fig. 1. Structure of stretchable electronic skin. (a) Schematic diagram of satellites used to location. (b) Schematic diagram of the stretchable electronic skin. (c) Optical image of the stretchable electronic skin on the coordinate paper, which shows excellent transparency. (d) SEM image of the microstructures on PDMS film. Scale bar, 100 μm. (e) SEM image of the CNT-PDMS composite electrode. Scale bar, 2 μm.

non-developable surface due to the intrinsic stretchable characteristic of its components (that is, carbon nanotube and poly(dimethylsiloxane) composite (CNT-PDMS) electrodes, and microstructured PDMS film), and is self-powered based on the conjunction of triboelectrification and electrostatic induction. Inspired by Global Positioning System (GPS), as shown in Fig. 1(a), three satellites enable the positioning of the latitude and longitude coordinates (except for altitude information) for a location on Earth through GPS. Similarly, this analog electronic skin only utilizes three-point electrodes to minimize the number of electrical connections, reduce the terminal number, simplify the structure, and avoid the complicated fabrication procedure of the electrode [12], [17], [19], [20]. Based on the voltage ratios of three electrodes, the touch position is still located with millimeter precision resolution both on the flat and curvilinear surfaces. What's more, the signals used in positioning are generated by the triboelectric mechanism, which makes the electronic skin active and entirely self-powered.

II. Results and Discussion

A. Fabrication and Working Principles

The electronic skin has only one-layer structure, which is microstructured PDMS film with a thickness of 105 μm, working as the substrate and friction surface. Three CNT-PDMS composite point electrodes are patterned on the PDMS surface, as shown in Fig. 1(b). The distance between any two point electrodes is 5 cm, so three point electrodes form a regular triangle. So far, the number of electrodes in our design is least. The less electrode number means the less fabrication cost, further difficulties on electrode extraction, and in particular, less signal interference and data processing, which are indispensable for electronic skin being integrated with more and more functions. When it comes to fabrication, our device is suitable for fabricating in the large area with low cost and high yield, just putting the electrodes

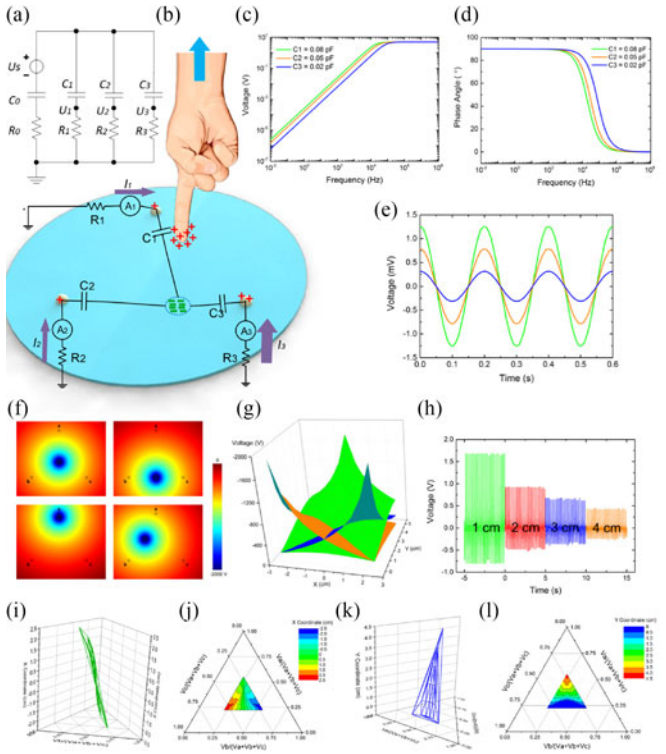

Fig. 2. Working principle and simulations of stretchable electronic skin. (a) Equivalent circuit model of electronic skin. (b) Charge distribution when finger contacts PDMS film and schematic diagram of the equivalent circuit when the finger moves. (c) Amplitude-frequency characteristic of three electrodes. In low-frequency region, the ratio of electrode voltages is dominated by capacitances. And at high frequency, the ratio is 1. (d) Phase frequency characteristic of three electrodes. With the increase of frequency, the phase shifts of electrode voltages become different. (e) Waveforms of three electrode voltages under the frequency of 5 Hz, the experiment frequency. (f) FES results of voltage distribution under different touch location (surface charge location). (g) FES result of the relationship between voltage amplitudes of the electrodes and touch location. (h) Voltages output of one electrode when the distance between the electrode and touch location increases from 1 cm to 4 cm. The positive peak voltage is inversely proportional to the distance approximately. (i) FES result of the relationship between normalized voltages points in a ternary diagram and x coordinate. (j) Two-dimension projection of (i) in a ternary diagram. (k) FES result of the relationship between normalized voltages points in a ternary diagram and y coordinate. (l) Two-dimension projection of (k) in a ternary diagram.

on the substrate directly and waiting for curing, no need for photolithography. The remarkable transparency of PDMS film enables clear observation of objects under the electronic skin. Fig. 1(c) gives an example of a coordinate paper under the electronic skin. The microstructured PDMS film is fabricated to enhance the triboelectric charge density when electronic skin contact with other objects (Fig. 1(d)). The CNT-PDMS composite is fabricated with the help of toluene and shows good uniformity (Fig. 1(e)) [35]–[37]. Because CNT-PDMS composite is a conductive elastomer, the electronic skin is stretchable and can be used on not only flat surface, but also curvilinear surface, such as the non-developable spherical surface.

When our finger or other object contacts the PDMS film surface, there are equal but opposite charges generated on the finger and electronic skin surface, which is known as triboelectrification (Fig. 2(b)) [22], [23]. At this time, the electrical field is confined in the space between finger and electronic skin

surface. When the finger moves away from the electronic skin, the negative charges on the PDMS film induce opposite charges on the three electrodes, which is called electrostatic induction. Because the distances between negative charges and electrodes are different, the amounts of induced positive charges on three electrodes are different (Fig. 2(b)). Therefore, different currents will come from the ground to each electrode when the finger moves away. Then, the charges on the electrodes will come back to the ground when finger with positive charges approaches the electronic skin. Therefore, different currents will flow back to the ground. The whole process is shown in Fig. S1. Considering the GPS positioning process, three point electrodes is enough to define two degrees of freedom location through analyzing the electrode voltages generated when finger departures or approaches the electronic skin.

After finger contacting the PDMS film, there will be some negative charges on the PDMS film surface and equal positive charge on the finger, the space between each electrode and negative charges on the PDMS film can be seen as a capacitor. When the distance between the electrode and negative charge on the PDMS film increases, the capacitance will decrease. The equivalent circuit model is displayed in Fig. 2(a). To investigate the relationship among electrodes' voltage, we derive the ratio among voltages under Kirchhoff's law. The detail is presented in the Note S1 and the result is shown as follow:

$$\begin{aligned}\dot{U}_1 : \dot{U}_2 : \dot{U}_3 = {} & [C_1R_1 + j\omega C_1R_1(C_2R_2 + C_3R_3) \\ & - \omega^2 C_1C_2C_3R_1R_2R_3] : [C_2R_2 + j\omega C_2R_2(C_1R_1 + C_3R_3) \\ & - \omega^2 C_1C_2C_3R_1R_2R_3] : [C_3R_3 + j\omega C_3R_3(C_2R_2 + C_1R_1) \\ & - \omega^2 C_1C_2C_3R_1R_2R_3] \end{aligned} \quad (1)$$

Where, $\dot{U}_1$, $\dot{U}_2$ and $\dot{U}_3$ are the phasor form and j is an imaginary unit. The result indicates that the ratio of electrode voltages depends on capacitance (C_1, C_2 and C_3), load resistance (R_1, R_2 and R_3) and frequency (ω).

According to the human body model [38], the human body is equal to a capacitor of 100 pF (C_0) and a resistor of 1.5 kΩ (R_0) connected in series. The capacitance between two points on a flat surface is as small as 0.01-0.1 pF according to our measurement. Therefore, C_1 is set to 0.08 pF, C_2 is set to 0.05 pF, C_3 is set to 0.02 pF. Specific values of C_1, C_2, C_3 are used to work as an example to help analyze the equivalent circuit model, frequency characteristics of the device and the relationship between capacitance and output voltage of electrodes. In fact, when touch location or structure of the electronic skin changes, the C_1, C_2, C_3 will change at the same time. It's very challenging to measure these capacities because the induced charges on the touch point cannot be extracted through an electrode or wire. However, it doesn't affect our position approach. Through experiments and calculation introduced below, the position sensitivity of the electronic skin stays at a high level no matter what surface the device attached.

The input voltage source is sine wave (5V) and the resistance of R_1, R_2 and R_3 are set to 100 MΩ. After analyzed by simulation program with integrated circuit emphasis (SPICE), frequency domain analysis results are provided. Amplitude frequency characteristics and phase frequency characteristics of three point electrodes are shown in Fig. 2(c) and (d), respectively. In the low-frequency region (less than 10 kHz), the voltage ratio among three electrodes stabilizes at 4.17: 2.57: 1, which is nearly to the radio of the three capacitance (4: 2.5: 1). When the capacitance becomes small, the equation can be simplified as $\dot{U}_1 : \dot{U}_2 : \dot{U}_3 \approx C_1 : C_2 : C_3$. When the frequency is less than 100 Hz, the phase shifts of all electrode voltages are about 90°. When frequency increases, the phase shifts of the voltages become different, which will cause different signal delay. Fig. 2(e) shows waveforms of U_1, U_2 and U_3 under the condition that the frequency of the input signal set to 5 Hz, which is equal to the frequency used in the experiment. We can see the radio of three electrode voltage is as same as above and all phase shifts are 90°.

Finite element simulation (FES) is used to calculate the voltage distributions with different touch locations. The results are shown in Fig. 2(f) and (g). When touch point moves, the negative charges (low potential) location on the PDMS film surface changes, voltages of all electrodes will change. In Fig. 2(f), the voltage of electrode *a* decreases and the voltages of electrodes *b* and c increase while touch point approaches electrode *a*. Fig. 2(g) presents the relationship between voltages of three electrodes and touch location (negative triboelectric charges region), the absolute value of open circuit voltage of one electrode will decrease quickly when the touch point moves away from the electrode, which can be explained by the equation:

$$U = -k\frac{Q}{r} \quad (2)$$

The absolute value of voltage (*U*) is inversely proportional to distance (*r*) between electrode and surface charges. Due to the symmetry, the open circuit voltage follows the same rule in every electrode. To verify the simulation, a vibration of 5 Hz is applied to the electronic skin surface under different touch location through a vibration generator system. The contact surface of the vibrator is a round PET film whose diameter is 5 mm. When the distance between the touch point and one electrode increases from 1 cm to 4 cm, the positive peak voltage of the electrode decrease from 1.68 V to 0.42 V (Fig. 2(h)), which shows similar tendency as the simulation result.

Every different touch point will cause different three electrodes' voltages, which means different voltages ratio. Therefore, it's convenient to normalize three voltages and locate it to a point in the ternary diagram. Fig. 2(i)-l display the FES results of the relationships between *x* and *y* coordinates and the normalized voltages ratio point in the ternary diagrams. They all show monotonicity, which is especially significant for positioning. We set the midpoint of electrode *b* and *c* as the origin of the coordinate, so the coordinate values of the electrode *a*, *b* and *c* are $(0, 5\sqrt{3}/2)$, $(-2.5, 0)$ and (2.5, 0), respectively. To locate the touch point, voltages of three electrodes generated by the touch are transferred to a point in the ternary diagram firstly, which is decided by the ratio of three voltages. Then the *x* and *y* coordinates are read out through figures. For example, in one test, the voltage of electrode *c* (V_c) is equal to the sum of voltage of the other two electrodes ($V_a + V_b$), and V_a is similar to V_b,

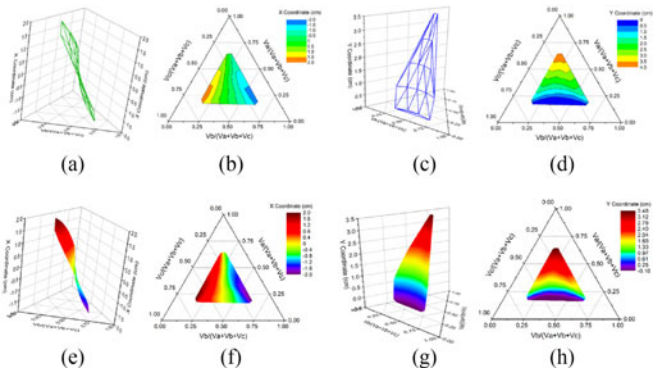

Fig. 3. Calibration results of the stretchable electronic skin when applied on the flat surface. (a) The relationship between normalized voltages point in ternary diagram and x coordinate based on 18 uniformly distributed test points. (b) Two-dimension projection of (a) in a ternary diagram. (c) Relationship between normalized voltages point in ternary diagram and y coordinate. (d) Two-dimension projection of (c) in a ternary diagram. (e) Fitting result of (a) calculated by interpolation and fitting algorithms. (f) Two-dimension projection of (e) in a ternary diagram. (g) Fitting result of (c) calculated by interpolation and fitting algorithms. (h) Two-dimension projection of (g) in a ternary diagram.

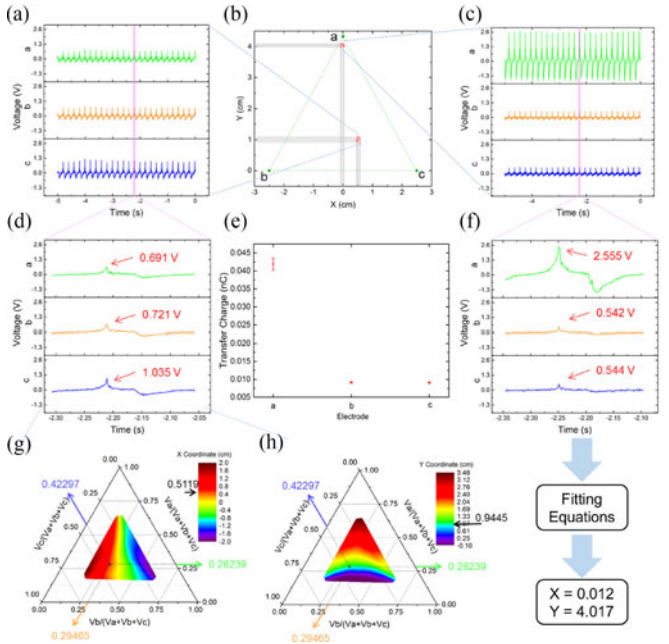

Fig. 4. Location ability of the stretchable electronic skin on the flat surface. (a) Voltage outputs of three electrodes when pressure applied to point (0.5, 1). (b) Coordinate calculation results of every group of voltage waveforms in (a) and (c). (c) Voltage outputs of three electrodes when pressure applied to point (0, 4). (d) One group of three electrode voltage outputs selected from (a) randomly. (e) Transfer charges of three electrodes when pressure is applied to point (0, 4). (f) One group of three electrode voltage outputs selected from (c) randomly. And the location process. (g) The x coordinate calculated from the voltage outputs in (d) with the help of calibration result. (h) The y coordinate calculated from the voltage outputs in (d) with the help of calibration result.

the corresponding point in the ternary diagram is (0.25, 0.25, 0.5), we can read out the x coordinate of touch point is $2 \sim 2.5$ cm through Fig. 2(j), the projection of Fig. 2(i), and y coordinate is $0 \sim 0.5$ cm through Fig. 2(l), the projection of Fig. 2(k). The method is so easy that we don't need complex data analysis if we get accurate ternary diagrams, just read out the coordinates.

B. Positioning Process of Electronic Skin Applied to Flat Surface

As a demonstration of the calibration process, 18 uniformly distributed points are chosen as the calibration points to obtain accurate ternary diagrams (Fig. S2). A vibration same as above is applied to the electronic skin, the contact surface is still a round PET film that is 5 mm in diameter, and the load resistance between each electrode and a reference ground is 100 MΩ. Fig. 3(a)–(d) show the calibration results based on 18 test points, which display the same tendencies with simulation results (Fig. 2(i)–(k). Because the region of x coordinate of 18 calibration points is from -2 to 2, the region of y coordinate is from 0 to $2\sqrt{3}$, some points on the electronic skin cannot be located through these figures, such as point $(-2.2, 0)$ or $(0, 4)$. Also, the resolution of the electronic skin is limited if we locate point through these figures directly. Adding more calibration points or performing interpolation can improve the resolution the smart skin. Herein, we insert extra points to each calibration ternary diagram through interpolation algorithm and then fit the point array with surface equations (the details are available in Note S2 and Note S3). After these process, the results are presented in Fig. 3(e)–(h), which are more suitable for positioning the touch point.

The electronic skin shows good stability and significant resolution on the flat surface based on the fitting ternary diagrams. 15 points are chosen as the test points to verify the location ability of electronic skin (Fig. S2). Fig. 4(a) presents the voltage waveforms of three electrodes when pressure is applied to point (0.5, 1). The voltage of electrode c is the largest, and voltage of electrode b is a little higher than the voltage of electrode a, which is corresponding to the distance relationships between touch point and each electrode. When touch point (0, 4) approaches electrode a, the voltage of electrode a is much higher than voltages of the other two electrodes, and voltage of electrode b is nearly equal to the voltage of electrode c (Fig. 4(c)), which agrees with the symmetry. There are some possible reasons for the variation of the output voltages. The first is the instability of the power amplifier and vibration driver, which may cause slight differences in the force applied to the electronic skin surface, the different forces may cause different outputs. The second is the electrostatic discharge (ESD) phenomena [39], which has been discovered in the triboelectric nanogenerator (TENG). In TENG, asymmetrical contact pairs introduce an unstable state, which causes a continuous surface charge increase and eventually the air breakdown, the output voltages are influenced by this process. The reason we choose positive peak voltages to locate is that they are more notable and stable, which is obvious in Fig. 4(c). The voltage ratios of data in Fig. 4(a) and (c) are gathered in point (0.287, 0.293, 0.420) and point (0.704, 0.149, 0.147), respectively (Fig. S3). For each group of three voltages, a location point (red circle) is calculated through ternary diagrams or fitting equations and shown in Fig. 4(b). A group of three voltages is selected randomly from Fig. 4(a) and presented in Fig. 4(d). The positive peak voltages of electrode a, b and c are 0.691 V, 0.721 V and 1.035 V, respectively, which are then normalized and transferred

to the point (0.28239, 0.29465, 0.42297) in ternary diagrams of x and y coordinates. From Fig. 4(g), x coordinate corresponding to the point is 0.5119, and from Fig. 4(h), y coordinate is 0.9445, which are near to the touch point (0.5, 1) and the error sum of x and y coordinates for this test is 0.564 mm. Because the points electrodes located cannot be chosen as calibration points, there must be some points between electrodes and calibration points, whose coordinates are excluded from ternary diagrams, (0, 4) is such a point. Fig. 4(f) presents a group of voltages selected from Fig. 4(c) randomly. The positive peak voltages of electrodes *a*, *b* and *c* are 2.555 V, 0.542 V and 0.544 V, respectively, which are then inputted to the fitting equations to calculate the coordinates. The result is (0.012, 4.017), and the error sum for this test is 0.29 mm. Fig. S4 shows the average error sums of all 15 test points based on 25 groups waveforms of each test, the whole data can be found in Table S1. The maximum of error sum is 1.593 mm and the minimum is just 0.211 mm, which shows our analog electronic skin has excellent positioning ability when applied on the flat surface.

The induced charge on PDMS is the critical factor in determining sensitivity. We calculate the amounts of transfer charge of three electrodes when pressure is applied to the point (0, 4) on the flat surface condition through integrating currents, the result is shown in Fig. 4(e). Point (0, 4) is chosen because the distance between the touch point and electrode *b* and *c* is greatest and touch point is closest to electrode *a*, as shown in Fig. 4(b), whose results are representative. For a certain induced charges on the substrate after one touch, the farther the distance between induced charges and electrode is, the fewer charges will transfer between the electrode and ground according to the attenuation of the electric potential of induced charges. In this test, the mean transfer charges of the electrode *a*, *b* and *c* are 0.04187 nC, 0.00913 nC and 0.00907 nC, respectively. According to the electrostatic induction, the amount of charge induced by triboelectrification should not less than 0.06007 nC in one touch. However, influenced by electrostatic discharge, dielectric materials and electromagnetic environment, the actual value of the induced charge is difficult to calculate accurately. Theoretically, there is no limit of charge required for measurement. As long as there is induced charge, output voltages will be generated on the electrodes. However, for the accuracy limitation of the detection equipment and the interference of ambient noise, the charge required for measurement in our experiment should reach $\sim$1 pC order, in which condition, the output voltages of the electrode *b* and *c* reduce to several 10 mV (calculated by scale), which is in the same order with the ambient noise. Microstructure and some chemistry methods could help to increase the amount of induced charge through enhancing the contact areas. It also cannot be ignored that the required induced charges could decrease by improving the accuracy of the detection device or testing in the environment with small ambient noise.

C. Positioning Process of Electronic Skin Applied to Curvilinear Surface

To fully mimic the properties of skin, stretchability of the electronic skin is important and indispensable. Here, CNT-PDMS composite is fabricated as the electrode material on its excellent stretchability and conductivity. Therefore, the whole electronic skin is stretchable and can conformably contact with a curvilinear surface. Fig. 5(a) compares the resistances of three electrodes when electronic skin stretched in one direction in different degrees, the whole process could be seen in Fig. S5. The resistances of electrodes are still kept at 10 kΩ order. Because each electrode is connected to the reference ground through oscilloscope's probes with a load resistance of 100 MΩ, compared with the fixed load resistor, the influence on output voltages of the increase of the electrode resistance ($\sim$10 kΩ) caused by strain is negligible. Then, the electronic skin stretched 30% in one direction is attached on a cylindrical surface (diameter = 7.5 cm), which also has two degrees of freedom and thus is suitable for our electronic skin to positioning. 18 uniformly distributed points are chosen as the calibration points and the results of the calibration and fitting after the same process introduced above are shown in Fig. 5(b) and (c) and Note S4 in the supporting information, which seems less smooth than Fig. 3(f) and (h), but has the same tendency. The reasons are that the shape of three electrodes has changed to an irregular triangle (Fig. 5(d)), and the capacitances between induced charges on the touch point and electrodes are influenced not only the distances but also the dielectric materials. Fig. 5(e) shows the output voltage waveforms when pressure is applied to point (0.5, 2), after normalizing the voltage ratios of output data, the location results are displayed in Fig. 5(f).

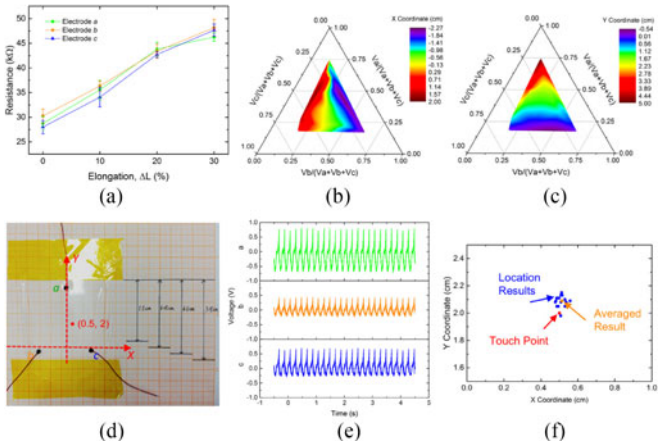

Fig. 5. Location ability of the electronic skin on the cylindrical surface. (a) The resistance of three electrodes when the electronic skin stretched in one direction in different degrees. Fitting results of (b) x coordinate and (c) y coordinate after calibration, interpolation and fitting processes. (d) Optical image of electronic skin stretched 30% in one direction on the flat surface. (e) Voltage outputs of three electrodes when pressure applied to point (0.5, 2). (f) Each blue dot's coordinates are calculated from a group output voltages of three electrodes from (e), orange dot is the averaged result of all the groups, and the red dot's coordinates is the touch point.

Besides cylindrical surface, the electronic skin could be attached to the non-developable surface when it stretched in more than one direction, such as spherical surface (Fig. 6(a)). The stretchable electronic skin shows significant positioning ability when attached to the spherical glass surface for the first time. The voltage distributions with different touch location are

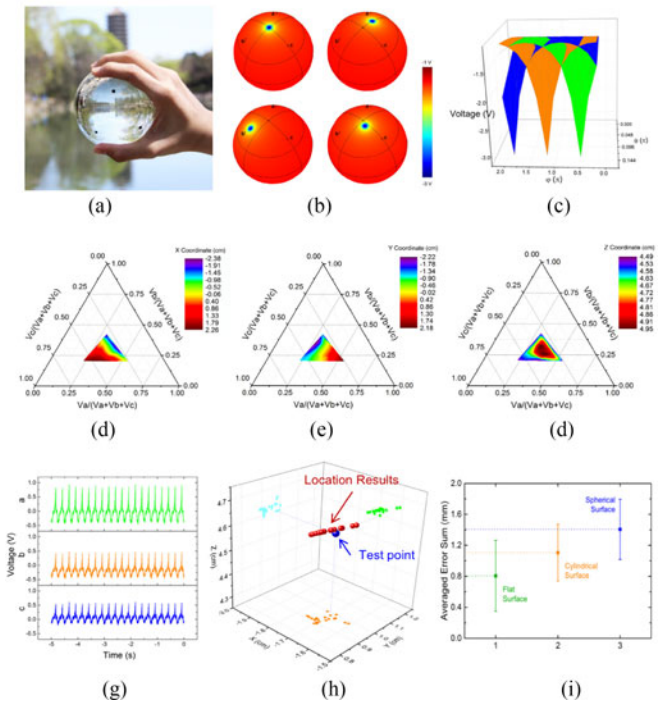

Fig. 6. Location ability of the stretchable electronic skin on the spherical surface. (a) Optical image of the stretchable electronic skin on a spherical glass surface, which shows excellent stretchability and transparency. (b) FES results of voltage distribution under different touch location (surface charge location) on spherical surface. (c) FES result of the relationship between voltage amplitudes of the electrodes and touch location in the spherical coordinate system. (d) Fitting result of the relationship between normalized voltages point in ternary diagram and x coordinate. (e) Fitting result of the relationship between normalized voltages point in ternary diagram and y coordinate. (f) Fitting result of the relationship between normalized voltages point in ternary diagram and z coordinate. (g) Voltage outputs of three electrodes when pressure applied to spherical surface point ($\varphi = 150^\circ$ ($x = -1.6970$, $y = 0.9798$), $z = 4.6$). (h) Coordinate calculation results (red ball) of every group of voltage waveforms in (g), blue ball is the position applied pressure. (i) Averaged error sums calculated from six groups' output voltages gathered in different days of the electronic skin attached on flat, cylindrical and spherical surfaces, respectively.

calculated by FES (Fig. 6(b) and (c)). As same as the flat condition above, the voltage of electrode b decreases and the voltages of electrodes a and c increase while touch point approaches electrode b (Fig. 6(b)). Ignoring altitude, the position of the object on Earth can be determined by three GPS satellites. Similarly, for the radius of the sphere is defined ($r = 5$ cm), the points on the spherical surface have only two degrees of freedom, and the position can be determined by voltages of three electrodes. Fig. 6(c) presents the relationship between voltages of three electrodes and touch location characterized in the spherical coordinate system (Fig. S6). There are three wave peaks in Fig. 6(c), the absolute value of open circuit voltage of one electrode will increase quickly when touch point (negative triboelectric charges region) approaches electrodes. Although the voltage distributions are influenced by glass sphere, not just the distances between electrodes and touch point, and not as regular as flat condition, they are still suitable to be used to positioning for the obvious distinctions among voltages of three electrodes for each touch. 19 points on the electronic skin are chosen as calibration points (Table S2). In this case, the spherical coordinate system is replaced by the spatial rectangular coordinate system, the center of the spherical is set as the origin (Fig. S6). After fitting, the results are shown in Fig. 6(d)–(f) and Note S5 in the supporting information. Similar to Figs. 3(f), (h), 6(d) and (e) both show good monotonicity. In Fig. 6(f), from edge to center, the color translates from violet to red, which means z coordinate increases gradually, which is corresponding to the tendency that the closer touch point approaches center of electronic skin, the closer voltages of three electrodes become to each other. To contact the spherical surface conformably, the electronic skin must be stretched, so the distribution of three electrodes are not geometrically symmetric absolutely. Therefore, the ternary diagrams also are influenced, become irregular and less symmetry. Fig. 6(g) presents the waveforms of three electrodes when pressure applied to one test point (blue ball), for each group of three voltages, a location result (red ball) is calculated through ternary diagrams and shown in Fig. 6(h). Fig. S7 chooses one group of three voltages from Fig. 6(g) and explains the positioning process, the error sum is 0.433 mm, which shows the significant location ability of the electronic skin on the spherical surface.

In order to verify the stability of the device under different conditions, six groups output voltages have been gathered in different days, then the error sums are calculated and compared with the averaged values, as shown in Fig. 6(i). All touch positions are located with millimeter precision resolution no matter what the shapes of surfaces are. The difference in error sums is according to the different sensitivities and accuracies when electronic skin applied on various surfaces. The sensitivity is highest when electronic skin applied to the flat surface, then decreases when applied to the cylindrical, and finally, is lowest when applied to the spherical surface, which is also displayed obviously when we compare the calibration and fitting results under different conditions (Figs. 3(f), (h), 5(b) and (c) and 6(d)–(f)). The fitting result of the flat surface is smoother than the curvilinear surface. The smoothness of the surface could be seen relevant to the sensitivity and accuracy.

Another advantage of this electronic skin is that there is no limitation of the substrate. Except for PDMS, we also test Solaris (Smooth-on, Macungie, Pennsylvania, PA, USA), a stretchable and transparent silica gel, as the substrate. There is no microstructure on the surface and the distance between electrodes increase to 10 cm, the electronic skin still works well (Fig. S8). Because the voltage is inversely proportional to the distance between electrode and surface charges approximately, the voltage will become more and more difficult to detect when the distance between electrode and touch point increases. Compared with all other electronic skin, this design is low-cost and simple fabrication with high yield, which makes it promising to be used in practice.

III. Conclusion

In summary, we introduced a new generation stretchable, transparent and self-powered analog electronic skin based on stretchable CNT-PDMS composite electrodes, which is low-cost and easy to fabricate in large scale. The design enables many

different materials to be used as the substrate with no limitation to intrinsically stretchable materials and triboelectric-favorable materials, which not only extends the applicability of this smart skin from the flat surface to any curvilinear surfaces but also provides ways to realize self-powered position sensing. Inspired by GPS, the configuration with minimum three electrodes simplifies the testing and fabrication processes. Except for the excellent performance when applied to the flat surface, the electronic skin also can be attached to cylindrical and spherical surfaces and give accuracy location. Based on triboelectrification and planar electrostatic induction, the electronic skin is entirely self-powered. For the simple structure and excellent properties, the electronic skin could be integrated with other functions, such as pressure and touch area detection, shows enormous potential in human/machine interaction and artificial intelligence.

APPENDIX

The Supporting Information is available.

REFERENCES

[1] A. Chortos, J. Liu, and Z. Bao, "Pursuing prosthetic electronic skin.," *Nature Mater.*, vol. 15, no. 9, pp. 937–950, 2016.

[2] J. E. O'Doherty *et al.*, "Active tactile exploration using a brain-machine-brain interface," *Nature*, vol. 479, no. 7372, pp. 228–231, 2011.

[3] M. L. Hammock, A. Chortos, B. C. Tee, J. B. Tok, and Z. Bao, "25th anniversary article: The evolution of electronic skin (e-skin): a brief history, design considerations, and recent progress.," *Adv. Mater.*, vol. 25, no. 42, pp. 5997–6038, 2013.

[4] J. Park, M. Kim, Y. Lee, H. S. Lee, and H. Ko, "Fingertip skin–inspired microstructured ferroelectric skins discriminate static/dynamic pressure and temperature stimuli.," *Sci. Adv.*, vol. 1, no. 9, 2015, Art. no. e1500661.

[5] C. Larson *et al.*, "Highly stretchable electroluminescent skin for optical signaling and tactile sensing," *Science*, vol. 351, no. 6277, pp. 1071–1074, 2016.

[6] D. Son *et al.*, "Multifunctional wearable devices for diagnosis and therapy of movement disorders," *Nature Nanotechnol.*, vol. 9, no. 5, pp. 397–404, 2014.

[7] D.-H. Kim *et al.*, "Epidermal electronics," *Science*, vol. 333, no. 6044, pp. 838–843, 2011.

[8] W. Gao *et al.*, "Fully integrated wearable sensor arrays for multiplexed in situ perspiration analysis," *Nature*, vol. 529, no. 7587, pp. 509–514, 2016.

[9] S. Krishnan, "Multimodal epidermal devices for hydration monitoring," *Microsyst. Nanoeng.*, vol. 3, 2017, Art. no. 17014.

[10] C. S. Boland *et al.*, "Sensitive electromechanical sensors using viscoelastic graphene-polymer nanocomposites," *Science*, vol. 354, no. 6317, pp. 1257–1260, 2016.

[11] H. Chen *et al.*, "Omnidirectional bending and pressure sensor based on stretchable CNT-PU Sponge," *Adv. Functional Mater.*, vol. 27, no. 3, 2017, Art. no. 1604434.

[12] C. C. Kim, H. H. Lee, K. H. Oh, and J. Y. Sun, "Highly stretchable, transparent ionic touch panel," *Science*, vol. 353, no. 6300, pp. 682–687, 2016.

[13] J. Kim *et al.*, "Stretchable silicon nanoribbon electronics for skin prosthesis," *Nature Commun.*, vol. 5, 2014, Art. no. 5747.

[14] T. Takahashi, K. Takei, A. G. Gillies, R. S. Fearing, and A. Javey, "Carbon nanotube active-matrix backplanes for conformal electronics and sensors," *Nano Letters*, vol. 11, no. 12, pp. 5408–5413, 2011.

[15] H. Lee *et al.*, "A graphene-based electrochemical device with thermoresponsive microneedles for diabetes monitoring and therapy," *Nature Nanotechnol.*, vol. 11, no. 6, pp. 566–572, 2016.

[16] J. Xu *et al.*, "Highly stretchable polymer semiconductor films through the nanoconfinement effect," *Science*, vol. 355, no. 6320, pp. 59–64, 2017.

[17] M. Shi *et al.*, "Self-powered analogue smart skin," *ACS Nano*, vol. 10, no. 4, pp. 4083–4091, 2016.

[18] K. Hu *et al.*, "Self-powered electronic skin with biotactile selectivity," *Adv. Mater.*, vol. 28, no. 18, pp. 3549–3556, 2016.

[19] X. Z. Jiang, Y. J. Sun, Z. Fan, and T. Y. Zhang, "Integrated flexible, waterproof, transparent, and self-powered tactile sensing panel," *ACS Nano*, vol. 10, no. 8, pp. 7696–704, 2016.

[20] M. S. Sarwar, Y. Dobashi, C. Preston, J. K. Wyss, S. Mirabbasi, and J. D. W. Madden, "Bend, stretch, and touch: Locating a finger on an actively deformed transparent sensor array," *Sci. Adv.*, vol. 3, no. 3, 2017, Art. no. e1602200.

[21] X.-S. Zhang, M.-D. Han, B. Meng, H.-X. Zhang, "High performance triboelectric nanogenerators based on large-scale mass-fabrication technologies," *Nano Energy*, vol. 11, pp. 304–322, 2015.

[22] F.-R. Fan, Z.-Q. Tian, and Lin Wang Z., "Flexible triboelectric generator," *Nano Energy*, vol. 1, no. 2, pp. 328–334, 2012.

[23] B. Meng *et al.*, "A transparent single-friction-surface triboelectric generator and self-powered touch sensor," *Energy Environ. Sci.*, vol. 6, no. 11, 2013, Art. no. 3235.

[24] W. Wu *et al.*, "Piezoelectricity of single-atomic-layer MoS2 for energy conversion and piezotronics," *Nature*, vol. 514, no. 7523, pp. 470–474, 2014.

[25] M. Han *et al.*, "R-Shaped hybrid nanogenerator with enhanced piezoelectricity," *Acs Nano*, vol. 7, no. 10, pp. 8554–8560, 2013.

[26] Z. L. Wang, "Triboelectric nanogenerators as new energy technology for self-powered systems and as active mechanical and chemical sensors," *ACS Nano*, vol. 7, no. 11, pp. 9533–9557, 2013.

[27] X. S. Zhang *et al.*, "Frequency-multiplication high-output triboelectric nanogenerator for sustainably powering biomedical microsystems," *Nano. Lett.*, vol. 13, no. 3, pp. 1168–1172, 2013.

[28] Kenry, J. C. Yeo, and C. T. Lim, "Emerging flexible and wearable physical sensing platforms for healthcare and biomedical applications," *Microsyst. Nanoeng.*, vol. 2, 2016, Art. no. 16043.

[29] X. Cheng *et al.*, "Implantable and self-powered blood pressure monitoring based on a piezoelectric thinfilm: Simulated, in vitro and in vivo studies," *Nano Energy*, vol. 22, pp. 453–460, 2016.

[30] Y. Song *et al.*, "Integrated self-charging power unit with flexible supercapacitor and triboelectric nanogenerator," *J. Mater. Chem. A*, vol. 4, no. 37, pp. 14298–14306, 2016.

[31] X. Cheng *et al.*, "Controlled fabrication of nanoscale wrinkle structure by fluorocarbon plasma for highly transparent triboelectric nanogenerator," *Microsyst. Nanoeng.*, vol. 3, 2017, Art. no. 16074.

[32] X. Chen *et al.*, "A wave-shaped hybrid piezoelectric and triboelectric nanogenerator based on P (VDF-TrFE) nanofibers," *Nanoscale*, vol. 9, no. 3, pp. 1263–1270, 2017.

[33] X. Pu *et al.*, "Eye motion triggered self-powered mechnosensational communication system using triboelectric nanogenerator," *Sci. Adv.*, vol. 3, no. 7, 2017, Art. no. e1700694.

[34] J. Chen *et al.*, "A self-powered 2D barcode recognition system based on sliding mode triboelectric nanogenerator for personal identification," *Nano Energy*, vol. 43, pp. 253–258, 2018.

[35] S.-J. Woo, J.-H. Kong, D.-G. Kim, and J.-M. Kim, "A thin all-elastomeric capacitive pressure sensor array based on micro-contact printed elastic conductors," *J. Mater. Chem. C*, vol. 2, no. 22, 2014, Art. no. 4415.

[36] S. Pyo *et al.*, "Development of a flexible three-axis tactile sensor based on screen-printed carbon nanotube-polymer composite," *J. Micromech. Microeng.*, vol. 24, no. 7, 2014, Art. no. 075012.

[37] L. Wang *et al.*, "PDMS/MWCNT-based tactile sensor array with coplanar electrodes for crosstalk suppression," *Microsyst. Nanoeng.*, vol. 2, 2016, Art. no. 16065.

[38] N. Cho, J. Yoo, S.-J. Song, J. Lee, S. Jeon, and H.-J. Yoo, "The human body characteristics as a signal transmission medium for intrabody communication," *IEEE Trans. Microw. Theory Tech.*, vol. 55, no. 5, pp. 1080–1086, May 2007.

[39] Z. Su, M. Han, X. Cheng, H. Chen, X. Chen, and H. Zhang, "Asymmetrical triboelectric nanogenerator with controllable direct electrostatic discharge," *Adv. Functional Mater.*, vol. 26, no. 30, pp. 5524–5533, 2016.

Authors' photographs and biographies not available at the time of publication.